ARTICLES

Experimental and Theoretical Studies on the Intramolecular Charge-Transfer Emission of Phenyldisilanes

Masataka Yamamoto, Takako Kudo, Mitsuo Ishikawa,† Seiji Tobita, and Haruo Shizuka*

Department of Chemistry, Gunma University, Kiryu, Gunma 376-8515, Japan

Received: September 16, 1998; In Final Form: January 13, 1999

Fluorescence and its polarization spectra of phenylpentamethyldisilane (**1**) and its para-substituted derivatives (para-substituent: $-C(CH_3)_3$ (**2**), $-OCH_3$ (**3**), and $-N(CH_3)_2$ (**4**)) were measured in a poly(vinyl alcohol) film at 77 K. Intramolecular charge transfer (ICT) fluorescence together with locally excited (LE) emission was found even for the compounds having an electron-donating substituent at the para-position (**2** and **3**) as well as that of **1**. The ICT state of these compounds showed an in-plane long axis polarization. By the measurements of fluorescence lifetimes, it was found that there was no dynamic equilibrium between the ICT and LE states, indicating that the ICT state originates from the nonrelaxed excited singlet ($S_n^\dagger$) state. Ab initio MO calculations (CASSCF and MRMP methods) were performed for the ground and excited states of phenyldisilane with planar and perpendicular conformations. The following results were obtained: (1) upon excitation, the ICT of phenyldisilane occurs from the phenyl moiety to the disilanyl group regardless of planar or perpendicular conformation, (2) in the course of the ICT formation, conformational changes in the Si−dimethyl group adjacent to the phenyl group play an important role rather than a twisting motion of the disilanyl group, and (3) the ICT state consists of the π,π'^* state produced by ICT from the phenyl moiety to the disilanyl group, where π'^* denotes the excited pseudo-π orbital.

1. Introduction

The photophysics and photochemistry of organosilicon compounds has become an interesting field in chemistry.[1−20] The dual (locally excited (LE) and intramolecular charge transfer (ICT)) emission of phenylpentamethyldisilane (**1**) was found in 1981[1] as a noticeable photophysical property of organosilicon compounds. The ICT fluorescence has a broad and structureless band with a large Stokes shift.[1,2,4] Picosecond laser flash photolysis experiments of **1** showed that (1) the ICT state was produced in less than 10 ps upon excitation, even in rigid glass at 77 K, and (2) the rearranged silene at 425 nm was formed with a buildup time of 30 ps after excitation in nonpolar media at 293 K, which was equal to the decay time of the ICT fluorescence of **1**, showing that the rearranged silene originated from the ICT state of **1**.[6−8] Leigh and Sluggett[16] carried out the nanosecond laser photolysis experiments of 1,1,1-trimethyltriphenyldisilane. They found that the corresponding rearranged silene was produced within a time scale shorter than the duration of the excitation pulse, while the homolytic fission of the Si−Si bond of phenyldisilanes was revealed to occur from the triplet state.

Since the discovery of the dual fluorescence of (4-dimethylamino)benzonitrile (DMABN) in a variety of solvents,[21] dual emission of organic molecules has attracted a great deal of interest.[22−31] The compounds which exhibit dual emission include aromatic amines as represented by DMABN, arylanilines, biaryls, dye systems, stilbenoid systems, etc. For these compounds, a number of studies have been devoted primarily to clarify the structural changes of the solute molecule and the role of solvent in the course of the ICT state formation. Until recently, a variety of different models were proposed to explain the dual emission of the above compounds. In the case of DMABN and its related compounds, it has been revealed that almost full charge migration occurs from the dimethylamino group to the phenyl ring in the ICT state. The occurrence of such charge separation was originally attributed to the twisting of the dimethylamino group with respect to the benzene ring, resulting in the formation of the so-called "twisted intramolecular charge transfer" (TICT) state.[32] Recently, Zachariasse et al.[33] proposed an alternative model called the "planar intramolecular charge transfer" (PICT) model. In this model the relaxed CT state is considered to have an essentially planarized structure, with a less pyramidal amino nitrogen atom and different bond lengths than in the LE state, resulting in a larger dipole moment.

Phenyldisilenes can be regarded as another class of compounds showing dual fluorescence in solution, and the formation mechanism of the ICT state is of great interest. The fluorescence polarization measurements of **1** in EPA glass at 77 K showed that the ICT state has an in-plane long-axis polarization.[7] We proposed the in-plane type ICT mechanism that was ascribed to the ($2p\pi^*$,$3d\pi$, or σ^*) state produced by the $2p\pi^*$(benzene ring) to vacant $3d\pi$ (Si−Si bond) intramolecular charge-transfer transition without twisting or internal rotation.[1−8] On the other hand, Sakurai et al. proposed the orthogonal intramolecular

† Department of Chemical Technology, Kurashiki University of Science and the Arts, Kurashiki, Okayama 712, Japan.

10.1021/jp983731i CCC: $18.00
Published on Web 04/08/1999

CHART 1

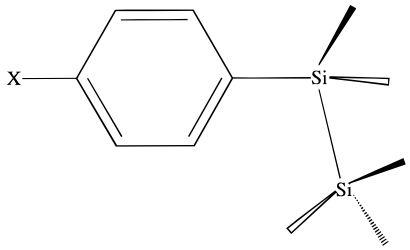

1: X= H
2: -C(CH$_3$)$_3$
3: -OCH$_3$
4: -N(Me)$_2$

charge transfer (OICT) mechanism[10,12] in which the charge transfer was assumed to occur from the σ(Si−Si) orbital to the vacant π orbital of the benzene ring, resulting in the (σ(Si−Si), 2pπ*(benzene)) state. The $^1(\sigma,2p\pi^*)$ state thus formed was considered to be stabilized by twisting or internal rotation of the disilanyl group with respect to the phenyl ring to form an orthogonal electronic structure. A similar mechanism was also proposed for phenylethynylpentamethyldisilanes by Horn et al.[9]

Numerous experimental considerations on the ICT mechanism of **1** came from the large dependence of the ICT fluorescence of **1** on the substituent, especially in para-substituted compounds. Fluorescence measurements of some para-substituted compounds of **1** in several solvents were carried out by Sakurai et al.[10] They reported that the para-substituted compounds having an electron-donating group, such as (4-methoxyphenyl)pentamethyldisilane and [4-(*N*,*N*-dimethylamino)phenyl]pentamethyldisilane, gave no ICT emission, even in polar solvents, and that for para-substituted compounds with an isopropenyl group, (4-isopropenylphenyl)pentamethyldisilane, ICT emission was detected even in nonpolar solvents. Tajima et al.[20] reported ICT fluorescence from 4-cyanophenylpentamethyldisilane (CPDS) having a strong electron-accepting substituent at the para-position in a supersonic molecular beam. From the observation of ICT fluorescence of CPDS in an isolated molecular condition, they proposed that the ICT emission of **1** originated from the charge-shifted state from the disilanyl group to the phenyl group. However, the electronic structure of CPDS is considered to be modified significantly from that of **1** because of the presence of a strong electron-accepting cyano group.

Recently, we found a large enhancement of the ICT emission of **1** in PVA film at 77 K.[13,15] In the present work, we carried out the fluorescence measurements of (4-*tert*-butylphenyl)-pentamethyldisilane (**2**), (4-methoxyphenyl)pentamethyldisilane (**3**), and [4-(*N*,*N*-dimethylamino)phenyl]pentamethyldisilane (**4**) along with **1** in PVA film at 77 K in order to confirm the existence of ICT fluorescence in these compounds having an electron-donating group at the para-position. So far a few theoretical studies on the ICT process for phenyldisilanes have been reported.[7,19] To obtain more insight into the ICT mechanism for **1**, ab initio calculations were also performed in the present study. The results of the calculations present a theoretical basis for understanding of electronic structures of the ICT state.

2. Experimental Section

2.1. Materials. Phenylpentamethyldisilane (**1**),[34] (4-*tert*-butylphenyl)pentamethyldisilane (**2**),[35] (4-methoxyphenyl)pentamethyldisilane (**3**),[36] and [4-(*N*,*N*-dimethylamino)phenyl]-pentamethyldisilane (**4**)[36] were prepared as reported in the literature. Compounds **1**, **2**, **3**, and **4** (as shown in Chart 1) were purified by column chromatography. An EPA mixture comprising ether, isopentane, and alcohol in a ratio of 5:5:2 was used.

Poly(vinyl alcohol) (PVA) (99% hydrolyzed, molecular weight (MW), 89000−98000) was obtained from Aldrich. PVA films were obtained by a method described in the literature.[37,38] The sample films were obtained by immersing the PVA films in a solution of methylcyclohexane containing ca. 5×10^{-3} M samples of **1**−**4** for 24 h at room temperature (RT).

2.2. Methods. Absorption spectra were recorded on a Jasco Ubest-50 spectrophotometer. The fluorescence and its polarization spectra were taken with a Hitachi M850 spectrofluorometer. The degree of polarization (P) was calculated by the following equation

$$P = \frac{I_{||} - fI_{\perp}}{I_{||} + fI_{\perp}} \quad (1)$$

where $I_{||}$ and $I_{\perp}$, respectively, denote the fluorescence intensities when the electric vectors of fluorescence are parallel and perpendicular to that of the excitation light and f is a correction factor for the polarization of the apparatus used.

The fluorescence lifetime was obtained with a time-correlated single-photon counting fluorometer (Edinburgh Analytical Instruments, FL900CDT).

2.3. Theoretical Calculations. The basic wave functions mainly used in this work were of the multiconfigurational self-consistent filed (MCSCF) type. In particular, the approach used here was that commonly referred to as fully optimized reaction space (FORS)[39] or complete active space SCF (CASSCF).[40] The fundamental idea was to identify those orbitals and electrons that participated in the photophysical processes of **1**, add the corresponding antibonding orbitals, and then consider the resulting set of *m* orbitals and *n* electrons as comprising an active space. A CASSCF wave function from this CASSCF(*n*,*m*) active space was constructed from a variationally optimized linear combination of all electronic configurations that could be obtained by distributing the *n* active electrons among the *m* active orbitals. For CASSCF calculations of phenyldisilane (PDS) and phenyldimethyldisilane (DMPDS), (6,6) active space was used. For the LE state, the six orbitals are the benzene (π,π*), Si−Si bonding, and their antibonding orbitals. For the ICT state, on the other hand, the six orbitals are the benzene (π,π*), Si−Si and C−Si bonding, and their antibonding orbitals.

Geometry optimizations were carried out at the HF/3-21G* or CASSCF(6,6)/3-21G* level. Final energies for PDS and DMPDS were obtained with second-order multireference perturbation theory (MRMP)[41] and CASSCF(6,6)/6-31G* at the CASSCF/3-21G* geometries. These single-point MRMP calculations were performed using the 3-21G* and 6-31G* standard basis sets. Calculations were performed using the GAMESS[42] and Gaussian 94[43] suite of programs on an IBM RS/6000 workstation (model 41T).

3. Results and Discussion

3.1. Experimental Findings. *3.1.1. Absorption and Emission Spectra.* The absorption and emission spectra of compounds **1**−**4** in EPA at 300 and 77 K are shown in Figure 1. It has been reported that compound **1** gives dual fluorescences originating from LE and ICT excited states (e.g., at around 3.4 $\times$ 10^4 (LE) and 2.9 $\times$ 10^4 cm^{-1} (ICT) in cyclohexane) in various solvents at RT.[4] The fluorescence spectra of **1** in EPA at 300 K (Figure 1a, dashed line) also show the ICT emission at around 3.0 $\times$ 10^4 cm^{-1} together with the weak LE one at 3.5 $\times$ 10^4 cm^{-1}. On the other hand, the fluorescence spectra of **2**−**4** in

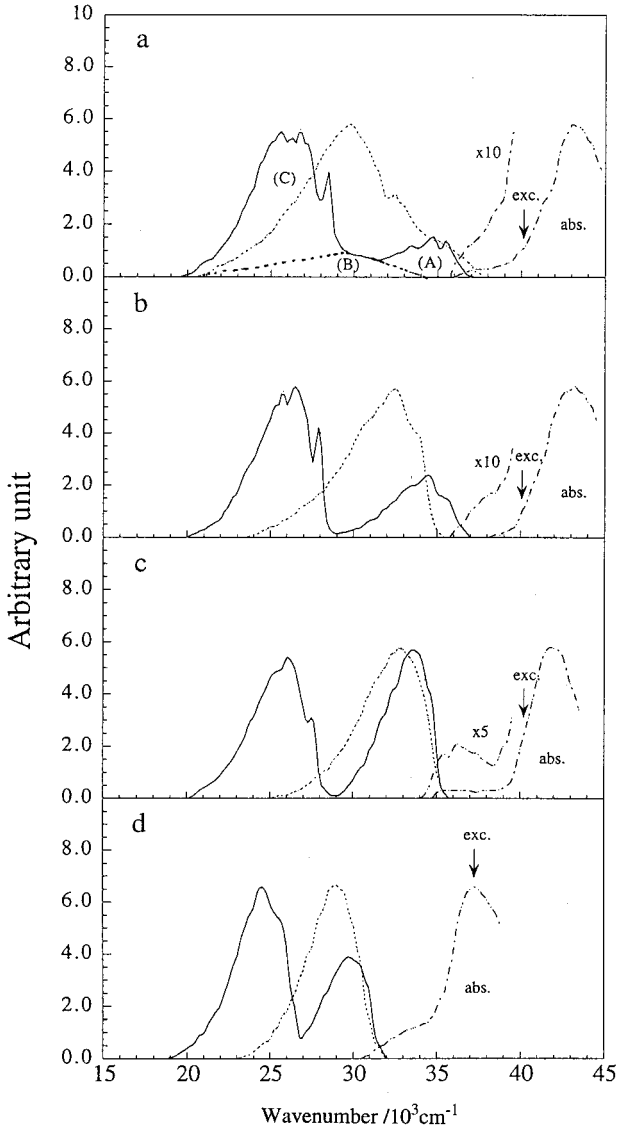

Figure 1. Absorption ((−•−) at 300 K) and fluorescence ((- - -) at 300 K; (—) at 77 K) spectra of **1** (a), **2** (b), **3** (c) (λ_{ex} = 250 nm), and **4** (d) (λ_{ex}= 270 nm) in EPA, where A, B, and C are LE, ICT, and phosphorescence spectra, respectively.

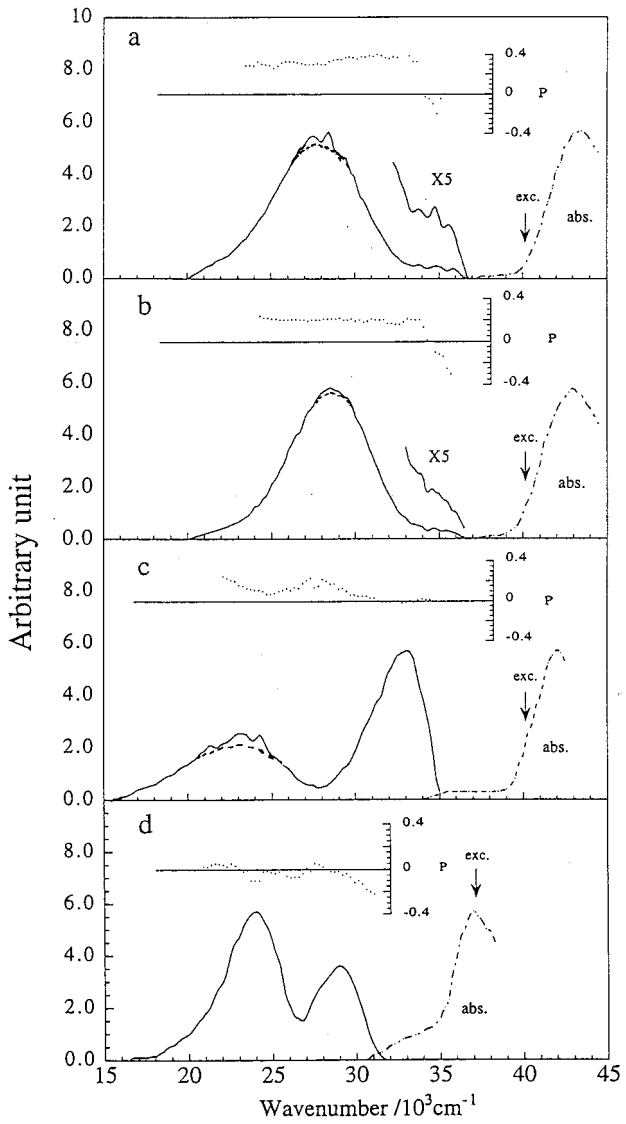

Figure 2. Absorption (−•−) and fluorescence (—) and fluorescence polarization (•••) spectra of **1** (a), **2** (b), **3** (c) (λ_{ex} = 250 nm), and **4** (d) (λ_{ex} = 270 nm) in PVA film at 77 K.

EPA at 300 K exhibit no ICT emission and consist almost entirely of the LE band. The emission spectra (solid line) of **1** in EPA glass at 77 K show three emission bands at around 3.5 × 10^4, 3.0 × 10^4, and 2.6 × 10^4 cm^{-1}, which are ascribable to fluorescences from LE (A) and ICT (B) excited states and phosphorescence (C), respectively. However, the emission spectra of **2**−**4** in EPA at 77 K give only two emission bands which can be assigned to LE fluorescence (shorter wavelength) and phosphorescence (longer wavelength). It should be noted here that no ICT emission was observed for compounds **2**−**4** with an electron-donating substituent at the para-position in EPA at RT as reported by Sakurai et al.[10]

As shown in Figure 2a in the next section, the intensity of the ICT emission of **1** was strongly enhanced in PVA film at 77 K. Therefore, we carried out the fluorescence measurements of **2**−**4** in PVA at 77 K whose ICT emission could not be observed even in rigid polar EPA glass at 77 K.

3.1.2. Fluorescence and Its Polarization Spectra in PVA Film at 77 K. Figure 2 shows the total emission spectra of **1**−**4** in PVA at 77 K and the degree of polarization (P) calculated by using eq 1. These spectra are obtained upon excitation at 250 nm (4.0 × 10^4 cm^{-1}) for **1**−**3** and excitation at 270 nm (3.7 × 10^4cm^{-1}) for **4**, which correspond to the $^1B_1 \leftarrow {}^1A_1$ (or $^1L_a \leftarrow {}^1A$) transition with in-plane long-axis polarization.[7]

Since the LE fluorescence of **1**−**3** would correspond to the $^1B_2 \rightarrow {}^1A_1$ (or $^1L_b \rightarrow {}^1A$) transition, the P values in the LE band are expected to be negative. In fact, in Figure 2 the LE emission bands (peak energies for **1**−**3** = 3.5 × 10^4, 3.5 × 10^4, and 3.3 × 10^4 cm^{-1}, respectively) show negative P values. The P value of the ICT emission of **1** has been shown to become positive.[7] The phosphorescence polarization spectra should also show negative P values under the experimental conditions, as reported previously.[7] Taking these facts into account, the broad emission bands at longer wavelengths (at 2.7 × 10^4 cm^{-1} (**1**), 2.8 × 10^4 cm^{-1} (**2**), and 2.3 × 10^4 cm^{-1} (**3**)) can be assigned to the ICT fluorescence. Very weak phosphorescence with vibrational structures is also observed at the peak of the ICT band for **1**−**3**. In contrast, the ICT emission of **4**, which may be superimposed on the phosphorescence band at 2.4 × 10^4 cm^{-1}, remains obscure. This may be due to the fact that a strong electronic conjugation between the amino group and the phenyl moiety may affect the electronic structures for **4**.

It can be said that compounds **2** and **3**, having a substituent with moderate electron-donating character, give the ICT fluo-

TABLE 1: Lifetimes (τ_f^{LE} and τ_f^{ICT}) of the ^{1}LE and ^{1}ICT Fluorescences and Phosphorescence Lifetime (τ_p) of 1, 2, and 3 in PVA Film at 77 K[a]

compound	τ_f^{LE} (ns)	τ_f^{ICT} (ns)	τ_p (ms)
1	21.9	4.2	78
	(34.3)[b]	(4.4)[b]	(81)[b]
2	16.4	6.9	116
3	7.1	4.2	95

[a] Errors within 5%. [b] In EPA at 77 K.

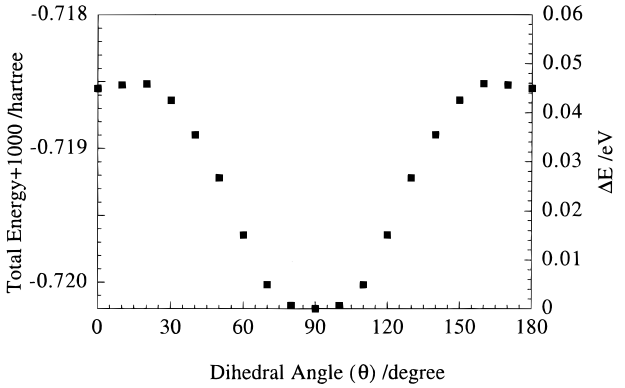

Figure 3. Calculated total energies of **1** as a function of the dihedral angle (Si1−Si2−C3−C4) shown in Chart 2. The calculations were performed by the HF/3-21G* method.

rescence with an in-plane long-axis polarization in PVA at 77 K as in the case of **1**. Since the ICT fluorescences of **1**−**3** were detected in PVA film at 77 K, we measured the fluorescence lifetimes of **1**−**3** in PVA at 77 K along with that of **1** in EPA at 77 K.

3.1.3. Fluorescence Lifetime. In Table 1, the lifetimes of the LE and ICT fluorescences and the phosphorescence lifetime are summarized for the compounds **1**−**3** in PVA film at 77 K. The ICT fluorescence lifetimes of **1**, **2**, and **3** in PVA film at 77 K are 4.2, 6.9 and 4.2 ns, respectively, which are similar to that (4.4 ns) of **1** in an EPA rigid matrix at 77 K. Therefore, the enhancement of the ICT emission in polar PVA film at 77 K is not attributable to an increase of the ICT lifetime but the large efficiency for the ICT state formation from the nonrelaxed excited singlet ($S_n^\dagger$) state, as discussed later (section 3.2.6). The radiationless processes competing with the ICT state formation may decrease in polar PVA film at 77 K. The reason the ICT emission of **1** is enhanced in PVA at 77 K remains unclear at present. The fluorescence lifetimes of the ICT state are different from those of the LE state having relatively long lifetimes (21.9 ns (**1**), 16.4 ns (**2**), and 7.1 ns (**3**)). These results indicate that no equilibrium between the LE and ICT states exists in the excited phenyldisilanes.

3.2. Theoretical Considerations on the ICT State Formation. *3.2.1. Ground-State Conformations of 1.* In Figure 3 the total energies of **1** in the ground-state calculated at the HF/3-21G* level are plotted as a function of the torsional angle. Here the torsional angle is taken as the dihedral angle (C4−C3−Si2−Si1) of the disilanyl group (see Chart 2). The free rotation around the C3−Si2 bond would be expected from the small energy difference (0.045 eV) between the planar and perpendicular conformers. In the case of PDS, a smaller energy difference (0.019 eV) was obtained by HF/3-21G* calculations, suggesting that the energy difference originates not only from steric repulsion due to the methyl groups but also from electronic interactions between the phenyl moiety and disilanyl group. Therefore, in the following CASSCF level calculations, the planar and perpendicular conformations having C_s symmetry

CHART 2

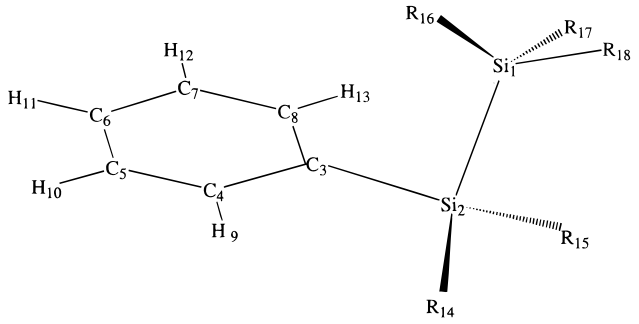

(**1**)

R_{14}-R_{18} :CH_3
R_{14}-R_{18} : H (PDS)
R_{14}, R_{15}:CH_3; R_{16}-R_{18} : H (DMPDS)

were employed as prototypical conformations for theoretical considerations.

3.2.2. Optimized Geometries of PDS and DMPDS in the S_0, LE, and ICT States. Because of restricted computing time, the constraint of C_s symmetry was maintained throughout all optimizations and the methyl groups in **1** were replaced by hydrogen atoms, i.e., phenyldisilane (PDS) was employed instead of **1** in the following CASSCF level calculations.

The optimized geometries for the two conformers (planar and perpendicular) of PDS in the ground (S_0), LE, and ICT states are obtained at the CASSCF(6,6)/3-21G* level as shown in Table 2. The ground-state geometry of PDS optimized at the CASSCF(6,6)/3-21G* level is in good agreement with that obtained by HF/6-31G** calculations reported for the perpendicular conformation.[19]

For the Franck−Condon excited singlet states (S_1−S_{10}), we performed second-order configuration-interaction (SOCI)[44] single-point calculations using the CASSCF wave function as the reference wave function and the CASSCF optimized ground-state geometries. It was found that all the excited singlet states (S_1−S_{10}) thus obtained corresponded to the LE state and no ICT states were involved. For the low-lying excited singlet state, we carried out CASSCF optimizations using the ground-state optimized geometries as a starting geometry. However, we could not find any ICT states. Therefore, we performed CASSCF calculations of the S_1 state by using modified starting geometries. Since it is expected that the ICT state formation is accompanied by significant structural changes in the disilanyl group, geometrical parameters in the disilanyl group (i.e., Si1−Si2 and Si2−C3 bond distances and Si1−Si2−C3 and C3−Si2−H14 bond angles) were modified. First, CASSCF calculations for PDS were carried out by using one of the above bond distances or bond angles as a geometrical parameter. The Si1−Si2 and C3−Si2 bond distances were changed in the range of 1.8−2.5 and 1.6−2.0 Å, respectively. Similarly, the Si1−Si2−C3 and C3−Si2−H14 bond angles were altered in the range of 90−120° and 90−120°. The result showed that geometrical changes in the C3−Si2−H14 bond angle play the most important role in stabilization of the ICT state. Therefore, geometry optimizations for the excited states were performed by using different C3−Si2−H14 bond angles between 90° and 120°.

In Table 2 the optimized geometries of planar and perpendicular PDS at the CASSCF(6,6)/3-21G* level are listed for the S_0, LE, and ICT states. The geometrical changes upon excitation to the LE state are found to occur mainly in the benzene moiety, because the LE state formation corresponds

TABLE 2: CASSCF(6,6)/3-21G* Optimized Geometries (Bond Lengths in Angstroms, Bond Angles in Degrees, and Dihedral Angles in Degrees) for Planar and Perpendicular PDS and DMPDS in the S_0, LE, and ICT States

	planar			perpendicular		
	S_0	LE	ICT	S_0	LE	ICT
			PDS			
bond lengths						
Si1−Si2	2.373	2.372	2.368	2.384	2.357	2.370
C3−Si2	1.881	1.858	2.005	1.879	1.865	2.153
C4−C3	1.386	1.491	1.460	1.403	1.450	1.452
C5−C4	1.393	1.427	1.390	1.391	1.434	1.371
C6−C5	1.388	1.352	1.390	1.383	1.430	1.420
C6−C7	1.396	1.423	1.449	1.383	1.430	1.420
C7−C8	1.388	1.477	1.344	1.391	1.434	1.37
C8−C3	1.408	1.482	1.439	1.403	1.450	1.452
Si2−H14	1.480	1.481	1.559	1.478	1.479	1.507
bond angles						
Si1−Si2−C3	112.70	112.33	110.14	112.14	112.17	90.48
C3−C4−C5	121.46	121.06	121.82	120.89	121.22	121.61
C4−C5−C6	119.31	122.45	119.31	120.13	120.31	119.90
C5−C6−C7	119.65	121.48	119.91	120.08	119.59	120.43
C6−C7−C8	119.92	119.60	121.21	120.13	120.31	119.90
C7−C8−C3	121.01	120.17	121.15	120.89	121.22	121.61
C8−C3−C4	118.01	115.29	116.61	117.88	117.34	116.55
H14−Si2−C3	109.81	110.21	83.98	109.02	109.01	84.02
dihedral angles						
Si1−Si2−C3−C4	0.0	0.0	0.0	90.0	90.0	90.0
H14−Si2−C3−C4	121.48	121.62	99.07	210.89	210.79	208.25
			DMPDS			
bond lengths						
Si1−Si2	2.348	2.347	2.350	2.361	2.361	2.393
C3−Si2	1.887	1.867	2.061	1.892	1.873	2.154
C4−C3	1.387	1.492	1.462	1.404	1.451	1.457
C5−C4	1.391	1.428	1.390	1.391	1.435	1.371
C6−C5	1.388	1.353	1.390	1.382	1.430	1.397
C6−C7	1.395	1.423	1.449	1.382	1.430	1.397
C7−C8	1.388	1.478	1.344	1.391	1.435	1.371
C8−C3	1.409	1.484	1.443	1.404	1.451	1.457
Si2−C14	1.894	1.906	1.982	1.903	1.891	1.929
bond angles						
Si1−Si2−C3	110.60	109.82	101.70	108.10	110.22	90.69
C3−C4−C5	121.58	121.11	122.06	121.19	121.45	121.80
C4−C5−C6	120.06	122.43	119.30	120.18	120.33	119.93
C5−C6−C7	119.57	121.56	119.88	119.90	119.51	121.32
C6−C7−C8	119.88	119.52	121.20	120.18	120.33	119.93
C7−C8−C3	121.18	120.26	121.41	121.19	121.45	121.80
C8−C3−C4	117.73	115.12	116.13	117.37	116.94	115.32
C14−Si2−C3	109.52	109.51	84.70	110.11	109.90	90.01
dihedral angles						
Si1−Si2−C3−C4	0.0	0.0	0.0	90.0	90.0	90.0
C14−Si2−C3−C4	120.30	120.04	102.96	209.49	210.24	214.30

to local (π,π^*) transitions in the benzene ring. In the ICT state, the optimized geometries of both planar and perpendicular conformations are substantially different from those of the S_0 state. In particular, drastic changes occur in the bond angles and dihedral angles of the disilanyl group. In the case of planar conformation, substantial decreases in the H14−Si2−C3 bond angle (−25.8°) and H14−Si2−C3−C4 dihedral angle (−22.4°) are recognized for the ICT state (Figure 4a). In the perpendicular ICT state, geometrical changes take place in the H14−Si2−C3 (−25.0°) and Si1−Si2−C3 bond angle (−21.7°) (Figure 4b). These results suggest that structural changes of C3−Si2−X (X = H14, H15, Si1) bond angles would act as an important reaction coordinate in the ICT state formation as schematically shown in Figure 4. Optimized geometries were also calculated for planar and perpendicular DMPDS to examine the effect of methyl groups on the ICT state formation. The results are shown in Table 2. In a manner similar to the case of PDS, substantial decreases can be seen in the C14−Si2−C3 bond angles and C14−Si2−C3−C4 dihedral angle for the ICT state of planar DMPDS and in the Si1−Si2−C3 and C14−Si2−C3 bond angles for the ICT state of perpendicular DMPDS, although the steric hindrance due to the methyl groups seems to depress the bond angle changes to some extent.

*3.2.3. Formal Charges and Dipole Moments of PDS and **1** in the S_0, LE, and ICT States.* In Table 3 the formal charges of planar and perpendicular PDS are listed for the S_0, LE, and ICT states. Table 4 presents the dipole moments and formal charges (total formal charge on the disilanyl group) of PDS and **1** calculated at several different levels. According to the HF/3-21G* calculations of **1** in the ground state, the total formal charges of the disilanyl group for the planar and perpendicular conformations are obtained to be +0.55, showing that partial charge migration takes place from the disilanyl group to the benzene moiety. The ground-state dipole moments (μ_g) of **1** in planar and perpendicular conformations are 0.2 and 0.12 D, respectively. The relatively small ground-state dipole moments of **1** are probably due to the fact that the +I and −M effects of the substituent cancel each other.[4,10]

The CASSCF(6,6)/3-21G* calculations of planar PDS show the total formal charges of the disilanyl group in the ground

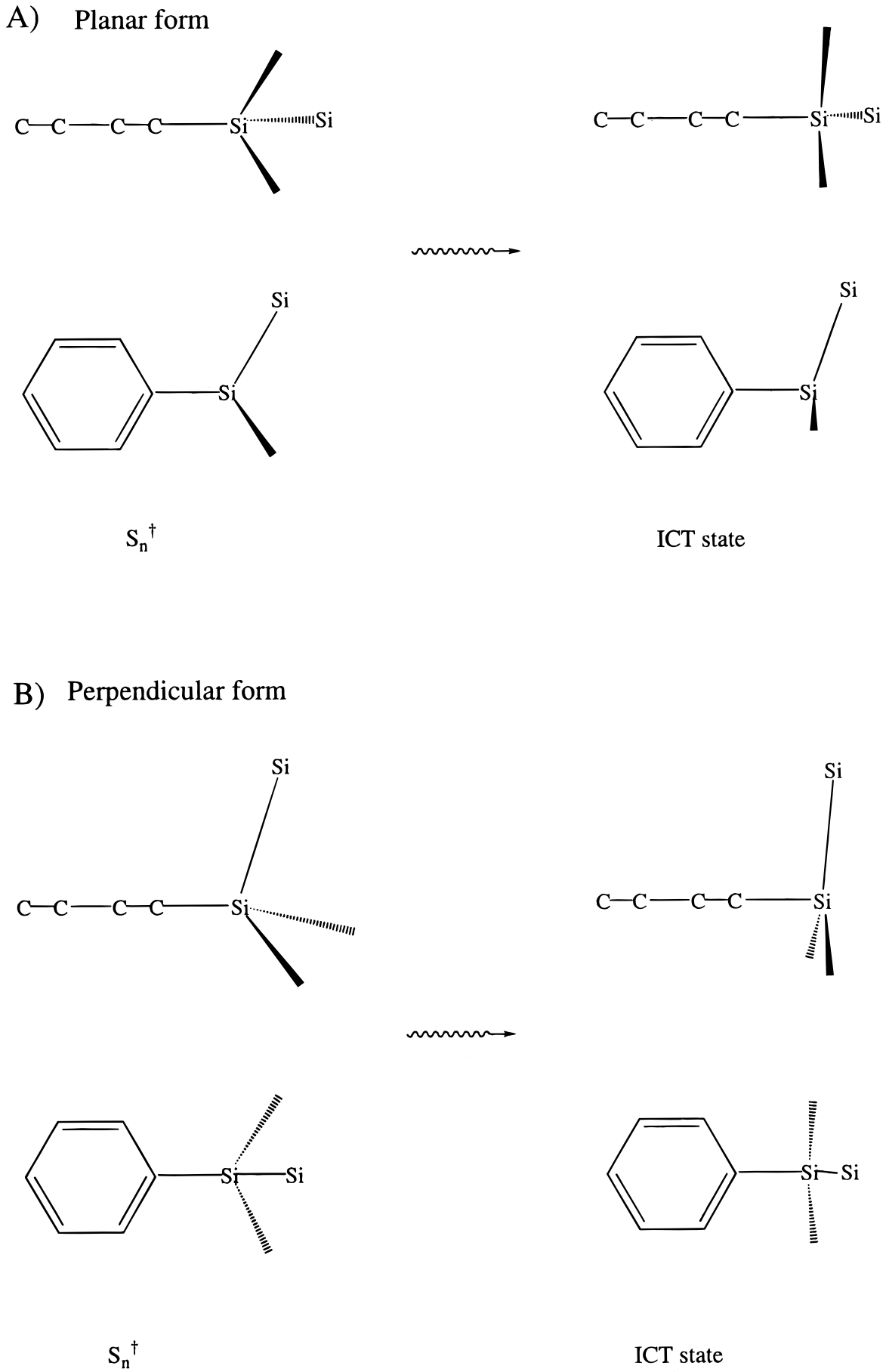

Figure 4. Schematic geometrical changes of PDS in the ICT formation. (A) Planar form. (B) Perpendicular form.

TABLE 3: Formal Charges of Planar and Perpendicular PDS in S_0, LE, and ICT States Obtained by CASSCF(6,6)/6-31G*//CASSCF(6,6)/3-21G* Calculations

	planar			perpendicular		
	S_0	LE	ICT	S_0	LE	ICT
Si1	+0.266	+0.267	+0.307	+0.288	+0.280	+0.295
Si2	+0.399	+0.408	+0.078	+0.373	+0.380	+0.114
C3	−0.147	−0.146	+0.034	−0.139	−0.151	−0.025
C4	−0.223	−0.229	−0.208	−0.215	−0.228	−0.211
C5	−0.190	−0.187	−0.193	−0.191	−0.175	−0.191
C6	−0.194	−0.203	−0.137	−0.201	−0.205	−0.121
C7	−0.186	−0.192	−0.174	−0.191	−0.175	−0.191
C8	−0.208	−0.212	−0.212	−0.215	−0.228	−0.211
H9	+0.206	+0.210	+0.268	+0.196	+0.198	+0.248
H10	+0.203	+0.201	+0.244	+0.201	+0.207	+0.237
H11	+0.201	+0.201	+0.255	+0.202	+0.208	+0.253
H12	+0.200	+0.208	+0.238	+0.201	+0.207	+0.237
H13	+0.201	+0.208	+0.255	+0.196	+0.198	+0.248
H14	−0.112	−0.114	−0.186	−0.107	−0.108	−0.159
H15	−0.112	−0.114	−0.186	−0.107	−0.108	−0.159
H16	−0.102	−0.103	−0.112	−0.101	−0.101	−0.110
H17	−0.102	−0.103	−0.112	−0.101	−0.101	−0.110
H18	−0.099	−0.100	−0.158	−0.092	−0.096	−0.145

(q_g) and LE states (q_e^{LE}) to be similar to each other (+0.31 and +0.32, respectively). In addition, the ground-state dipole moment ($\mu_g = 1.15$) changes to only a small extent after excitation to the LE state ($\mu_e = 1.07$). The results indicate that in the LE state substantial charge migration does not occur between the disilanyl group and the benzene moiety. A similar tendency is also seen for perpendicular PDS.

In a previous paper,[4] we reported the formation of a highly dipolar excited state for **1** in solvents having large dielectric constants, as revealed by a large solvatochromic shift of the fluorescence spectra. The difference in the dipole moment ($\mu_e - \mu_g$), where μ_g and μ_e denote the dipole moments of the ground and excited states, was estimated from the Lippert−Mataga equation.[45,46] By assuming the radius (a_0) of a spherical cavity containing the dipole to be 3.0 Å, the value of $\mu_e - \mu_g$ was obtained to be 4.4 D for **1**.[4] However, if we use the molecular volume defined as the volume inside a contour of 0.001 electrons/bohr^3 density, the cavity radius (a_0) of **1** is calculated to be 4.6 Å by using Gaussian 94 programs and one can obtain 8.3 D for $\mu_e - \mu_g$ for **1** from the Lippert−Mataga equation. That is, the value of μ_e is obtained to be 8.5 D.

On the other hand, the low-lying excited singlet states having a large dipole moment were found to be the ICT state of PDS by CASSCF level calculations using modified ground-state geometries as shown in the last column of Table 4. For instance, the calculated dipole moments ($\mu_e^{ICT} = 10.2$ and ~9.5 D for planar and perpendicular PDS) are found to be comparable to that (8.5 D) estimated by experiments. The total formal charges (q_e^{ICT}) of the disilanyl group of PDS in the ICT state become negative values (−0.23 and −0.18 for planar and perpendicular forms, respectively) compared to those in the ground state, showing that ICT occurs from the benzene moiety to the disilanyl group.

3.2.4. Orbital Characters of the LE and ICT States of PDS. The six orbitals included in the CASSCF(6,6) active space for the planar and perpendicular PDS in the LE and ICT states are depicted in Figures 5 and 6. In the LE state of the planar conformation (Figure 5A), the orbitals 36a″, 37a″, 38a″, and 39a″ represent the π orbitals of the benzene moiety while the 35a′ and 40a′ orbitals show the Si−Si bonding and Si−Si antibonding characters, respectively. In the LE state of the perpendicular conformation (Figure 6A), all six orbitals show π orbital character of the benzene moiety. These indicate that the LE states have mainly (π,π^*) character.

On the other hand, in the ICT state of the planar conformation (Figure 5B), not only the π orbitals in the benzene moiety (35a″, 37a″, and 40a″) but also the orbitals localized on the disilanyl group (36a′, 38a′, and 39a′) are included. It can be seen that the 38a′ orbital has its electron lobe on the Si2 atom. The CASSCF (6,6) active orbitals of the ICT state in the perpendicular conformation are depicted in Figure 6B. The orbitals 37a′ and 38a′ involve π orbitals of the benzene ring and also pseudo-π orbitals of the disilanyl group. Therefore, orbital characters of the ICT state having a planar or perpendicular conformation show that the charge-transfer state formation results from pseudo-π electronic interactions between the benzene ring and the disilanyl group. It can be said that the orbital characters of the ICT states for both planar and perpendicular conformations are consistent with the ICT emission having an in-plane long-axis polarization. That is, the ICT state can be regarded as a π,π'^* state, where π'^* denotes the pseudo π orbital included in the disilanyl group. The π'^* orbital mainly consists of 3p and 3d atomic orbitals of the Si atoms (orbital 38a′ for planar and perpendicular forms) as shown in Figure 5B and Figure 6B.

3.2.5. Energy Relationship. Total and relative energies for the ground and excited states of the planar and perpendicular PDS were calculated at CASSCF(6,6)/3-21G*, CASSCF(6,6)/6-31G*, MRMP/CASSCF(6,6)/3-21G*, and MRMP/CASSCF-(6,6)-/6-31G* levels as shown in Table 5. The lowest transition energy (ΔE) was obtained to be 4.6 eV from the 0−0 absorption band in cyclohexane.[4] All the calculated ΔE_{0-0} values in Table 5 show much higher energies compared to the experimental value (4.6 eV). The energy differences between the experimental and calculated ΔE_{0-0} values are significantly improved in MRMP calculations. It can also be seen that the energies of the geometry-optimized LE state (ΔE_{LE}) are smaller than ΔE_{0-0}, while the calculated energy levels of the ICT state are located slightly higher than ΔE_{0-0}.

Since the ICT fluorescence of **1** has not been observed in the gas phase,[11,20] one can expect that the stabilization due to solvation plays an important role in the ICT state formation. Therefore, we took solvation energies (ΔE_{solv}) in the ICT state into account by using the following equation.

$$\Delta E_{solv} = \frac{2\mu_e}{a_0^3}\left(\frac{\epsilon - 1}{2\epsilon + 1}\right) \qquad (2)$$

Here, it is assumed that the solvent molecules relax fully about a solute dipole within the lifetime of the excited state. In eq 2, μ_e, ϵ, and a_0 are the dipole moment in the excited state, the static dielectric constant of solvent, and the Onsager radius ($a_0 = 4.6$ Å for PDS). The excited-state energies in cyclohexane (CH, $\epsilon = 2.0$) and acetonitrile (MeCN, $\epsilon = 37.5$) were computed by adding the solvation energies to the corresponding excited-state energies of solvent-free systems. The ICT state in MeCN has a much smaller energy than ΔE_{0-0} at the CASSCF(6,6)/6-31G* level. Since the ICT states of planar and perpendicular PDS have large dipole moments (10.2 and 9.51 D, respectively), significant solvent-induced stabilization can be seen in polar MeCN. In nonpolar CH, the energy level of the ICT state is slightly smaller than ΔE_{0-0}.

The vertical transition energies (ΔE_f^{ICT}) for the fluorescence from the ICT state of PDS to the ground state in the gas phase in CH and MeCN were calculated as shown in parentheses in Table 5. The values of ΔE_f^{ICT} are significantly smaller than the vertical transition energies (ΔE_f^{LE}) for the local fluorescence because of the large Franck−Condon destabilization energy in

TABLE 4: Formal Charge (q) on the Disilanyl Group and Dipole Moment (μ in debye) in S_0, LE, and ICT States of PDS and 1 Calculated at the CASSCF and HF Levels[a]

conformation	compound	level of calculation	q_g	μ_g	q_e^{LE}	μ_e^{LE}	q_e^{ICT}	μ_e^{ICT}
planar	PDS	CASSCF(6,6)/3-21G*	+0.31	1.15	+0.30	1.07	−0.23	10.2
		CASSCF(6,6)/6-31G*//3-21G*	+0.14	1.11	+0.14	1.07	−0.37	10.2
	1	HF/3-21G*	+0.55	0.20				
perpendicular	PDS	CASSCF(6,6)/3-21G*	+0.32	0.97	+0.32	0.90	−0.18	9.55
		CASSCF(6,6)/6-31G*//3-21G*	+0.15	0.95	+0.15	1.68	−0.27	9.51
	1	HF/3-21G*	+0.55	0.12				

[a] q_e, q_e^{LE}, and q_e^{ICT} denote total formal charge on the disilanyl group in the ground, LE, and ICT states, respectively. μ_g, μ_e^{LE}, and μ_e^{ICT} are the calculated dipole moment in the ground, LE, and ICT states, respectively.

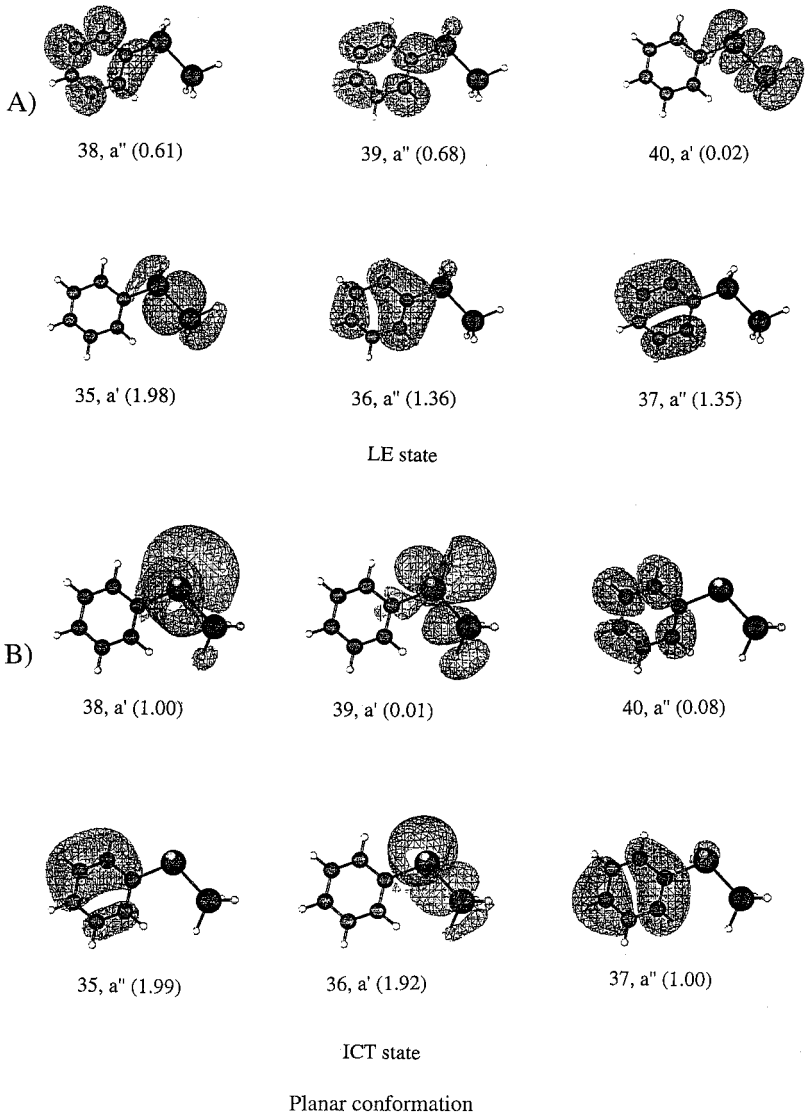

Figure 5. Six orbitals included in the CASSCF(6,6) active space for the LE (A) and ICT (B) states of the planar PDS. In parentheses, occupation numbers.

the ground state. The energy differences between the experimental and calculated ΔE_f values are significantly improved in MRMP/CASSCF(6,6)/6-31G* calculations.

3.2.6. Mechanism of the ICT State Formation. In this section, we consider the ICT emission mechanism of phenyldisilanes. Picosecond laser experiments showed that the rise time of the ICT emission was less than 10 ps, even in EPA rigid matrix at 77 K.[4] The dynamic equilibrium between the LE and ICT states of **1** is not established, as stated above. This result is in contrast with the dual emission of DMABN, where the dynamic equilibrium between LE and ICT is established because of the same value of their fluorescence lifetimes.[33]

Two possible mechanisms for the ICT emission of phenyldisilanes are considered. One is a mechanism where the LE or ICT state is produced upon excitation from the different ground-state conformation, e.g., planar or perpendicular conformation. The other is a mechanism where the production of the ICT state occurs via the nonrelaxed excited singlet ($S_n^\dagger$) state regardless of the ground-state conformation. The fluorescence measurements of both 1-trimethylsilyl-1-methyl-2,3-benzo-1-silacyclopentene having a perpendicular conformation and 1,1,2,2-tetramethyl-3,4-benzo-1,2-disilacyclopentene (or 1,1,2,2-tetramethyl-3,4-benzo-1,2-disilacyclohexene) having a planar or planar-like conformation in the ground state have shown that

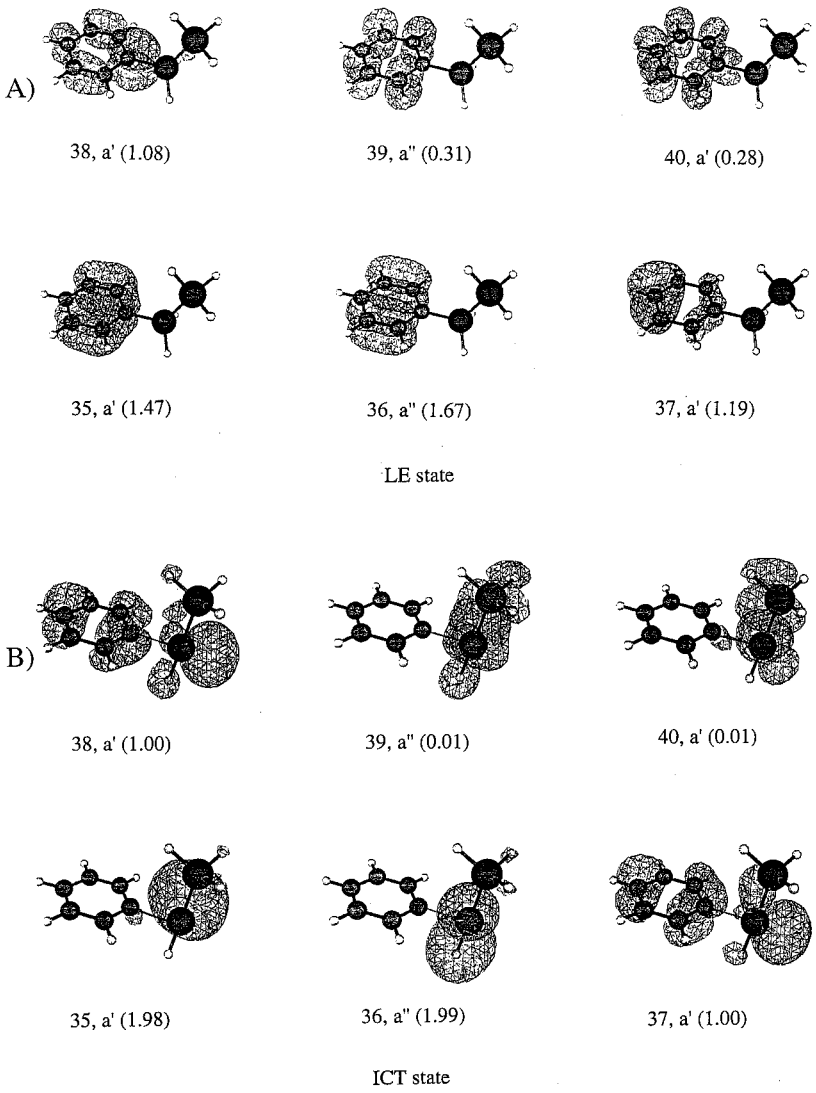

Figure 6. Six orbitals included in the CASSCF(6,6) active space for LE (A) and ICT (B) states of perpendicular PDS. In parentheses, occupation numbers.

TABLE 5: Calculated Total Energies (Hartrees) of the S_0 State and Energies (ΔE,[b] eV) of the Franck−Condon S_1, LE, and ICT States Relative in the S_0 State for the Planar and Perpendicular PDS[a]

					ΔE_{ICT}[b]		
compound	level of calculation	S_0	ΔE_{0-0}[b]	ΔE_{LE}[b]	in gas phase	in CH	in MeCN
planar PDS	CAS(6,6)/3-21G*	−806.7479	6.26	5.73 (5.20)	6.88 (3.75)	6.62 (3.49)	6.22 (3.09)
	MRMP/CAS(6,6)/3-21G*	−807.3835	5.10	4.87 (4.58)	6.39 (3.72)	6.13 (3.46)	5.73 (3.06)
	CAS(6,6)/6-31G*	−810.9079	6.24	5.72 (5.17)	6.29 (3/46)	6.03 (3.20)	5.63 (2.80)
	MRMP/CAS(6,6)/6-31G*	−811.7796	5.01	4.91 (4.46)	6.32 (3.96)	6.00 (3.55)	5.59 (3.15)
perpendicular PDS	CAS(6,6)/3-21G*	−806.7468	6.28	6.05 (5.47)	6.10 (3.76)	5.86 (3.52)	5.51 (3.17)
	MRMP/CAS(6,6)/3-21G*	−807.3823	5.24	4.78 (4.74)	6.33 (4.51)	6.09 (4.29)	5.75 (3.93)
	CAS(6,6)/6-31G*	−810.9073	6.12	4.08 (5.47)	6.33 (4.53)	6.10 (4.30)	5.75 (3.95)
	MRMP/CAS(6,6)/6-31G*	−811.7795	4.89	4.42 (4.23)	5.77 (3.76)	5.53 (3.52)	5.18 (3.17)
1	exp		4.60	(4.09)[c]		(3.64)[c]	(3.24)[c]

[a] All geometry optimizations are performed at the CASSCF(6,6)/3-21G* level. [b] ΔE_{0-0}, ΔE_{LE}, and ΔE_{ICT} denote the calculated energy differences between the ground (S_0) state and Franck−Condon S_1, LE, or ICT state, respectively. In parentheses, fluorescence energies calculated by ($\Delta E_f^{LE} = \Delta E_{LE} - \Delta E_{FC}^{LE}$) and ($\Delta E_f^{ICT} = \Delta E_{ICT} - \Delta E_{FC}^{ICT}$) are shown, where ΔE_{FC}^{LE} and ΔE_{FC}^{ICT} denote the Franck−Condon destabilization energies in the corresponding ground states. [c] Experimental values for the local fluorescence maximum energy in CH and the ICT fluorescence maximum energies in CH and in MeCN for **1** (see ref 4).

these compounds gave the ICT emission regardless their molecular conformation.[10] The results indicate that the conformation in the ground state is not so important for the ICT state formation. Therefore, the formation of the ICT state originates from the nonrelaxed $S_n^\dagger$ state regardless of the ground-state conformation. That is, the ICT state is produced by the intramolecular charge migration from the phenyl ring to the disilanyl group via the nonrelaxed $S_n^\dagger$ state upon excitation. A schematic presentation of the three states including the triplet state (T_1) is depicted in Figure 7.

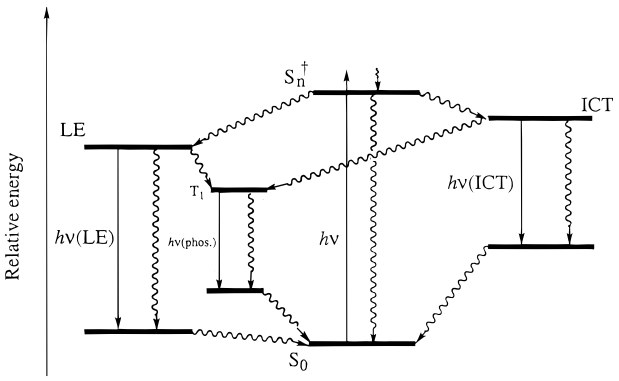

Figure 7. Schematic representation of the ground, LE, and ICT states of PDS: (—) radiative transition, (〰) radiationless transition. S_0 and $S_n^\dagger$ denote the ground and nonrelaxed excited singlet states, respectively. T_1 is the triplet state.

We reported that the ICT emission was very weak for 2,4,6-trimethylphenylpentamethyldisilane even in polar solvents.[2] This result showed that the methyl groups on the 2- and 6-positions play an important role for the restricted production of the ICT state of phenyldisilanes as shown in Figure 4. If the ICT state formation is mainly related to the conformational changes in the Si−dimethyl groups adjacent to the phenyl group, the methyl group on the ortho positions of the benzene ring are subject to steric repulsion by the methyl groups at the silicon atom adjacent to the benzene ring. As a result, the ICT emission of 2,4,6-trimethylphenylpentamethyldisilane would become very weak.

5. Summary

(1) From the measurements of the fluorescence and its polarization spectra in PVA film at 77 K, we found that the ICT emission together with the LE fluorescence could be detected for **2** (4-C$(CH_3)_3$) and **3** (4-OCH_3) having an electron-donating group, as in the case of **1**. The ICT emission of **1**−**3** showed an in-plane long-axis polarization. The enhancement of the ICT emission in polar PVA film at 77 K was attributable to an increase in the efficiency of the ICT state formation.

(2) The ICT fluorescence lifetimes of **1**−**3** were different from those of the LE state, demonstrating that there was no dynamic equilibrium between the ICT and LE states in these compounds. This implied that the ICT state was directly produced from the nonrelaxed excited singlet ($S_n^\dagger$) state.

(3) The calculations of ground-state optimized geometries for **1** showed that the energy barrier for internal rotation of the disilanyl group is relatively small (less than 0.05 eV). Although the perpendicular form was calculated to be the most stable conformer, the planar form was also predicted to exist as an equilibrium mixture.

(4) The geometry of the ICT state of PDS obtained by CASSCF(6,6)/3-21G* calculations suggested that the changes of C3−Si2−X bond angles are related to the ICT state formation. CASSCF(6,6) calculations of PDS showed that the intramolecular charge transfer occurs from the phenyl moiety to disilanyl group. The ICT state consisted of the π,π'^* state, where π'^* denotes the pseudo-π orbital included in the disilanyl group regardless of planar or perpendicular conformation. The π'^* orbital consists mainly of the 3p and 3d atomic orbitals of the Si atoms (orbital 38a′ for planar and perpendicular forms) as shown in Figures 5B and 6B.

(5) The results of CASSCF(6,6)/6-31G* calculations for PDS including solvation energy indicated that the ICT state formation from the nonrelaxed excited singlet ($S_n^\dagger$) state can become an exothermic process. The ΔE_f and ΔE_{0-0} values calculated at the MRMP/6-31G* level were in good agreement with the experimental data. The dipole moments of the ICT state (μ_e^{ICT} = 10.2 and 9.5 D for planar and perpendicular PDS, respectively) obtained by CASSCF(6,6)/6-31G* calculations showed reasonable agreement with the experimental value (μ_e = 8.5 D) based on the Lippert−Mataga equation.

Acknowledgment. The authors thank Prof. Keiji Morokuma of Emory University for his valuable comments and encouragements on the present study. We also thank Dr. Haruyuki Nakano of Tokyo University for many informative discussions about MRMP. This work was supported by a Grant-in-Aid on Priority-Area-Research: Photoreaction Dynamics (06239101) from the Ministry of Education, Science, and Culture of Japan.

References and Notes

(1) Shizuka, H.; Obuchi, H.; Ishikawa, M.; Kumada, M. *J. Chem. Soc., Chem. Commun*. **1981**, 405.
(2) Shizuka, H.; Sato, Y.; Ishikawa, M.; Kumada, M. *J. Chem. Soc., Chem. Commun*. **1982**, 439.
(3) Ishikawa, M.; Sugisama, H.; Fuchikami, T.; Kumada, M.; Yamabe, T.; Kawakami, H.; Fukui, K.; Ueki, Y.; Shizuka, H. *J. Am. Chem. Soc*. **1982**, *104*, 2872.
(4) Shizuka, H.; Sato, Y.; Ueki, Y.; Ishikawa, M.; Kumada, M. *J. Chem. Soc., Faraday Trans. 1* **1984**, *80*, 341.
(5) Shizuka, H.; Obuchi, H.; Ishikawa, M.; Kumada, M. *J. Chem. Soc., Faraday Trans. 1* **1984**, *80*, 383.
(6) Shizuka, H.; Okazaki, K.; Tanaka, M.; Ishikawa, M.; Sumitani, M.; Yoshihara, K. *Chem. Phys. Lett*. **1985**, *113*, 89.
(7) Hiratsuka, H.; Mori, Y.; Ishikawa, M.; Okazaki, K.; Shizuka, H. *J. Chem. Soc., Faraday Trans. 2* **1985**, *81*, 1665.
(8) Shizuka, H.; Okazaki, K.; Tanaka, H.; Tanaka, M.; Ishikawa, M.; Sumitani, M.; Yoshihara, K. *J. Phys. Chem*. **1987**, *91*, 2057.
(9) Horn, K. A.; Grossman, R. B.; Thorne, J. R. G.; Whitenack, A. A. *J. Am. Chem. Soc*. **1989**, *111*, 4809.
(10) Sakurai, H.; Sugiyama, H.; Kira, M. *J. Phys. Chem*. **1990**, *94*, 1837.
(11) Kira, M.; Miyazawa, T.; Mikami, N.; Sakurai, H. *Organometallics* **1991**, *10*, 3793.
(12) Sakurai, H.; Abe, J.; Sakamoto, K. *J. Photochem. Photobiol*. **1992**, *A65*, 111.
(13) Shizuka, H.; Hiratsuka, H. *Res. Chem. Interm*. **1992**, *18*, 131.
(14) Kira, M.; Miyazawa, T.; Sugiyama, H.; Yamaguchi, M.; Sakurai, H. *J. Am. Chem. Soc*. **1993**, *115*, 3116.
(15) Shizuka, H. *Pure Appl. Chem*. **1993**, *65*, 1635.
(16) Leigh, W. J.; Sluggett, G. W. *J. Am. Chem. Soc*. **1993**, *115*, 7531.
(17) Sluggett, G. W.; Leigh, W. J. *Organometallics* **1994**, *13*, 1005.
(18) Leigh, W. J.; Sluggett, G. W. *Organometallics* **1994**, *13*, 269.
(19) Ohshita, J.; Niwa, H.; Ishikawa, M.; Yamabe, T.; Yoshii, T.; Nakamura, K. *J. Am. Chem. Soc*. **1996**, *118*, 6853.
(20) Tajima, Y.; Ishikawa, H.; Miyazawa, T.; Kira, M.; Mikami, N. *J. Am. Chem. Soc*. **1997**, *119*, 7400.
(21) Lippert, E.; Lüder, W.; Moll, F.; Nägele, W.; Boos, H.; Prigge, H.; Seibold-Blankenstein, I. *Angew. Chem*. **1961**, *73*, 695.
(22) (a) Rotkiewicz, K.; Grellmann. K. H.; Grabowski, Z. R. *Chem. Phys. Lett*. **1973**, *19*, 315. (b) Rotkiewicz, K.; Grabowski, Z. R.; Krówczyński, A.; Kühnle, W. *J. Lumin*. **1976**, *12/13*, 877. (c) Rotkiewicz, K.; Rubaszewska, W. *Chem. Phys. Lett*. **1980**, *70*, 444. (d) Köhler, G.; Rechthaler, K.; Grabner, G.; Luboradzki, R.; Suwínska, K.; Rotkiewicz, K. *J. Phys. Chem. A* **1997**, *101*, 8518.
(23) For recent reviews, see: (a) Rettig, W. *Angew. Chem*. **1986**, *98*, 969. (b) Rettig, W. *Angew. Chem., Int. Ed. Engl*. **1986**, *25*, 971. (c) Rettig, W. In *Topics in Current Chemistry*; Mattay, J., Ed.; Springer-Verlag: Berlin, Heidelberg, 1994; Vol. 169, p 253 and references therein.
(24) LaFemina, J. P.; Duke, C. B.; Paton, A. *J. Chem. Phys*. **1987**, *87*, 2151.
(25) Majumdar, D.; Sen, R.; Bhattacharyya, K.; Bhattacharyya, S. P. *J. Phys. Chem*. **1991**, *95*, 4324.
(26) Hayashi, S.; Ando, K.; Kato, S. *J. Phys. Chem*. **1995**, *99*, 955.
(27) Serrano-Andrés, L.; Merchán, M.; Roos, B. O.; Lindh, R. *J. Am. Chem. Soc*. **1995**, *117*, 3189.
(28) Nordio, P. L.; Polimeno, A.; Saielli, G. *J. Photochem. Photobiol*. **1997**, *A105*, 269.
(29) Kim, H. J.; Hynes, J. T. *J. Photochem. Photobiol*. **1997**, *A105*, 337.
(30) Gedeck, P.; Schneider, S. *J. Photochem. Photobiol*. **1997**, *A105*, 165.
(31) (a) Sobolewski, A. L.; Domcke, W. *Chem. Phys. Lett*. **1996**, *250*, 428. (b) Sobolewski, A. L.; Domcke, W. *Chem. Phys. Lett*. **1996**, *259*, 119. (c) Sobolewski, A. L.; Domcke, W. *J. Photochem. Photobiol*. **1997**, *A105*,

325. (d) Sobolewski, A. L.; Sudholt, W.; Domcke, W. *J. Phys. Chem. A* **1998**, *102*, 2716.

(32) Grabowski, Z. R.; Rotkiewicz, K.; Siemiarczuk, A.; Cowley, D. J.; Baumann, W. *Nouv. J. Chim.* **1979**, *3* (7), 443.

(33) (a) Schuddeboom, W.; Jonker, S. A.; Warman, J. M.; Leinhos, U.; Kühnle, W.; Zachariasse, K. A. *J. Phys. Chem.* **1992**, *96*, 10809. (b) Zachariasse, K. A.; Haar, T.; Hebecker, A.; Leinhos, U.; Kühnle, W. *Pure Appl. Chem.* **1993**, *8*, 1745. (c) Zachariasse, K. A.; Haar, T.; Leinhos, U.; Kühnle, W. *J. Inf. Rec. Mats.* **1994**, *21*, 501. (d) Haar, T.; Hebecker, A.; II′ichev, Y. V.; Jiang, Y.-B.; Kühnle, W.; Zachariasse, K. A. *Recl. Trav. Chim. Pays-Bas* **1995**, *114*, 430. (e) Zachariasse, K. A.; Grobys, M.; Haar, T.; Hebecker, A.; II'ichev, Y. V.; Jiang, Y.-B.; Morawski, O.; Kühnle, W. *J. Photochem. Photobiol.* **1996**, *A102*, 59. (f) Zachariasse, K. A.; Grobys, M.; Haar, T.; Hebecker, A.; II′ichev, Y. V.; Morawski, O.; Rückert, I.; Kühnle, W. *J. Photochem. Photobiol.* **1997**, *A105*, 373. (g) II′ichev, Y. V.; Kühnle, W.; Zachariasse, K. A. *J. Phys. Chem. A* **1998**, *102*, 5670.

(34) Gilman, H.; Lichtenwalter, G. D. *J. Am. Chem. Soc.* **1958**, *80*, 608.

(35) Ishikawa, M.; Fuchikami, T.; Kumada, M. *J. Organomet. Chem.* **1977**, *133*, 19.

(36) Hevesi, L.; Dehon, M.; Cvutzen, R.; Lazarescu-Grigore, A. *J. Organomet. Chem.* **1997**, *62*, 2011.

(37) Tanizaki, Y. *Bull. Chem. Soc. Jpn.* **1959**, *32*, 75.

(38) Kawski, A.; Kubicki, A.; Kukliński, B. *J. Photochem. Photobiol.* **1993**, *A71*, 161.

(39) (a) Ruedenberg, K.; Sundberg, K. R. In *Quantum Science*; Calais, J.-L., Goscinski, O., Linderberg, J., Ohrn, Y., Eds.; Plenum Press: New York, 1976; pp 505−15. (b) Cheung, L. M.; Sundberg, K. R.; Ruedenberg, K. *J. Am. Chem. Soc.* **1978**, *100*, 8024. (c) Cheung, L. M.; Sundberg, K. R.; Ruedenberg, K. *Int. J. Quantum Chem.* **1979**, *16*, 1103. (d) Ruedenberg, K.; Schmidt, M. W.; Gilbert, M. M.; Elbert, S. T. *Chem. Phys.* **1982**, *71*, 41. (e) Ruedenberg, K.; Schmidt, M. W.; Gilbert, M. M. *Chem. Phys.* **1982**, *71*, 51. (f) Ruedenberg, K.; Schmidt, M. W.; Gilbert, M. M.; Elbert, S. T. *Chem. Phys.* **1982**, *71*, 65. (g) Feller, D. F.; Schmidt, M. W.; Ruedenberg, K. *J. Am. Chem. Soc.* **1982**, *104*, 960.

(40) (a) Roos, B. O. *Adv. Chem. Phys.* **1987**, *69*, 399. (b) Roos, B. O.; Taylor, P. R.; Shiegbahn, P. E. M. *Chem. Phys.* **1980**, *48*, 157. (c) Siegbahn, P. E. M.; Almlof, J.; Heiberg, A.; Roos, B. O. *J. Chem. Phys.* **1981**, *74*, 2384.

(41) (a) Hirao, K. *Chem. Phys. Lett.* **1992**, *190*, 374. (b) Hirao, K. *Chem. Phys. Lett.* **1992**, *196*, 397.(c) Hirao, K. *Chem. Phys. Lett.* **1993**, *201*, 59. (d) Hirao, K. *Int. J. Quantum Chem.* **1992**, *S26*, 517. (e) Nakano, H. *J. Chem. Phys.* **1993**, *99*, 7983. (f) Nakano, H. *Chem. Phys. Lett.* **1993**, *207*, 372.

(42) Schmidt, M. W.; Baldridge, K. K.; Boatz, J. A.; Elbert, S. T.; Gordon, M. S.; Jensen, J.; Koseki, S.; Matsunaga, N.; Nguyen, K. A.; Su, S. J.; Windus, T. L.; Dupuis, M.; Montogomery, J. A. *J. Comput. Chem.* **1993**, *14*, 1347.

(43) Frisch, M. J.; Trucks, G. W.; Schlegel, H. B.; Gill, P. M. W.; Johnson, B. G.; Robb, M. A.; Cheeseman, J. R.; Keith, T. A.; Petersson, G. A.; Montgomery, J. A.; Raghavachari, K.; Al-Laham, M. A.; Zakrzewski, V. G.; Ortiz, J. V.; Foresman, J. B.; Cioslowski, J.; Stefanov, B. B.; Nanayakkara, A.; Challacombe, M.; Peng, C. Y.; Ayala, P. Y.; Chen, W.; Wong, M. W.; Andres, J. L.; Replogle, E. S.; Gomperts, R.; Martin, R. L.; Fox, D. J.; Binkley, J. S.; Defrees, D. J.; Baker, J.; Stewart, J. P.; Head-Gordon, M.; Gonzalez, C.; Pople, J. A. *Gaussian 94*, Revision B.3; Gaussian, Inc.: Pittsburgh, PA, 1995.

(44) Schmidt, M. W.; Truong, P. N.; Gordon, M. S. *J. Am. Chem. Soc.* **1987**, *109*, 5217.

(45) (a) Lippert, E. *Naturforscher* **1955**, *10a*, 541. (b) Lipper, E. *Z. Elektrochem.* **1957**, *61*, 962.

(46) (a) Mataga, N.; Kaifu, Y.; Koizumi, M. *Bull. Chem. Soc. Jpn.* **1955**, *28*, 690. (b) Mataga, N.; Kaifu, Y.; Koizumi, M. *Bull. Chem. Soc. Jpn.* **1956**, *29*, 465.